



RESEARCH LETTER

10.1029/2020GL090139

Investigating Recent Changes in MJO Precipitation and Circulation in Multiple Reanalyses

Wei-Ting Hsiao¹ , Eric D. Maloney¹ , and Elizabeth A. Barnes¹ ¹Department of Atmospheric Science, Colorado State University, Fort Collins, CO, USA

Key Points:

- Non-monotonic changes in MJO circulation and precipitation amplitude over the period of 1981–2018 are found in ERA5 and MERRA-2
- A decrease in the ratio of MJO circulation to precipitation amplitudes is detected and can be explained by weak temperature gradient theory
- Examination of ERA-20C during 1901–2009 demonstrates similar ratio decreases before the satellite era

Supporting Information:

- Supporting Information S1

Correspondence to:

W.-T. Hsiao,
WeiTing.Hsiao@colostate.edu

Citation:

Hsiao, W.-T., Maloney, E. D., & Barnes, E. A. (2020). Investigating recent changes in MJO precipitation and circulation in multiple reanalyses. *Geophysical Research Letters*, 47, e2020GL090139. <https://doi.org/10.1029/2020GL090139>

Received 5 AUG 2020

Accepted 23 OCT 2020

Accepted article online 30 OCT 2020

©2020. The Authors.

This is an open access article under the terms of the Creative Commons Attribution License, which permits use, distribution and reproduction in any medium, provided the original work is properly cited.

Abstract Recent work using CMIP5 models under RCP8.5 suggests that individual multimodel mean changes in precipitation and wind variability associated with the Madden-Julian oscillation (MJO) are not detectable until the end of the 21st century. However, a decrease in the ratio of MJO circulation to precipitation anomaly amplitude is detectable as early as 2021–2040, consistent with an increase in dry static stability as predicted by weak temperature gradient balance. Here, we examine MJO activity in multiple reanalyses (ERA5, MERRA-2, and ERA-20C) and find that MJO wind and precipitation anomaly amplitudes have a complicated time evolution over the record. However, a decrease in the ratio of MJO circulation to precipitation anomaly amplitude is detected over the observational period, consistent with the change in dry static stability. These results suggest that weak temperature gradient theory may be able to help explain changes in MJO activity in recent decades.

Plain Language Summary A recent study examined future projected changes in precipitation and wind strength associated with the Madden-Julian oscillation (MJO) in a set of anthropogenically forced warming simulations. While they showed that changes in the amplitude of individual MJO-related variables are not detectable until the end of the 21st century, they also demonstrated that a decrease in the ratio of MJO wind to precipitation anomaly amplitude is detectable as early as 2021–2040. To examine whether these MJO changes found in climate models are realistic, changes to MJO variability are assessed in three observational products, and we find that a similar decrease in the ratio of MJO wind to precipitation strength is detectable over 1901–2018. The change in MJO activity is consistent with that expected under climate warming.

1. Introduction

The Madden-Julian oscillation (MJO; Madden & Julian, 1971, 1972) is the dominant mode of large-scale tropical precipitation variability on intraseasonal timescales. MJO activity impacts the occurrence of extreme weather events not only in tropics but also at higher latitudes due to its remote teleconnections (Zhang, 2013). Because of its ability to modulate weather across the globe, with clear implications for lives and property, extensive research is being conducted about the MJO, with increasing attention given to the evolution of the MJO under anthropogenic warming (Maloney et al., 2019). As global temperatures rise, MJO activity is expected to be impacted by competing effects, making the projections of the MJO difficult. For example, an increased basic state vertical moisture gradient in the lower troposphere increases the efficiency with which vertical motion moistens the atmosphere, leading to a strengthening of MJO-associated convection (Arnold et al., 2013; Holloway & Neelin, 2009). In contrast, an increased dry static stability decreases the efficiency by which diabatic heating induces vertical motion (Knutson & Manabe, 1995; Sherwood & Nishant, 2015; Sobel & Bretherton, 2000), which would tend to weaken MJO-associated convection (e.g., Chikira, 2014). Future projections from most global climate models (GCMs) suggest an increase in the amplitude of MJO precipitation under anthropogenic warming, although MJO circulation anomalies weaken, or at least increase less than precipitation (Maloney et al., 2019). Analysis of the reconstructed historical record from instrumental observations and reanalysis shows positive trends of MJO amplitude over the 20th century in surface pressure and precipitation (Oliver & Thompson, 2012) and in the late 20th century in zonal winds (Jones & Carvalho, 2006; Slingo et al., 1999). However, other studies have found no trend in boreal wintertime MJO amplitude from the 1980s to the 2000s when using an outgoing longwave radiation-related metric (Tao et al., 2015).

Recent evidence suggests that the MJO may undergo structural changes with warming and differences in intensification rate in its associated precipitation and circulation components. Such changes would be important because teleconnections generated by upper level divergence associated with MJO convection have a large impact on extratropical weather and its predictability (Ferranti et al., 1990; Zhang, 2013). Instead of examining the amplitude of the MJO with a single variable, Maloney and Xie (2013) and Wolding and Maloney (2015) suggest that in the deep tropics where the weak temperature gradient (WTG) approximation holds (Sobel & Bretherton, 2000), the amplitude ratio of vertical velocity to precipitation associated with the MJO is constrained by dry static stability. Since the temperature profile in the free tropical troposphere roughly follows a moist adiabat determined by convective adjustment in tropical convecting regions (Knutson & Manabe, 1995), the dry static stability profile may be constrained by future sea-surface temperature (SST) warming, thus providing a constraint on future MJO behavior.

A recent study found that the ratio of MJO-associated circulation to precipitation amplitude follows WTG balance in anthropogenic warming simulations (Bui & Maloney, 2019). The WTG approximation can be applied to the thermodynamic equation to produce the following approximate balance in the tropical free troposphere, where horizontal temperature gradients are small (Sobel & Bretherton, 2000),

$$\omega \frac{\partial s}{\partial p} \approx Q_1 \quad (1)$$

where ω is the vertical pressure velocity, s the dry static energy (DSE), and Q_1 the apparent heat source (Yanai et al., 1973). Note that all variables represent the large-scale area average. If it is further assumed that precipitation is proportional to Q_1 in MJO convective regions, and that the vertical structure of Q_1 is not changed (Maloney & Xie, 2013), it follows that at a given level,

$$\Delta \left(\frac{\omega}{P} \right) \propto \Delta \left(\frac{\partial s^{-1}}{\partial p} \right) \quad (2)$$

where P is the surface precipitation rate and Δ denotes the relative change from a reference state to a new state. Bui and Maloney (2019) examined GCM simulations forced by Representative Concentration Pathway 8.5 (RCP8.5) in a subset of models participating in the Coupled Model Intercomparison Project 5 (CMIP5) that simulated realistic MJOs. While the amplitude changes of MJO precipitation and vertical velocity were individually not detectable until 2080, the *ratio* of MJO vertical velocity to precipitation amplitude showed detectable decreases as early as 2021–2040. Consistent with WTG balance and the proportionality of precipitation to Q_1 , the ratio of MJO vertical velocity to precipitation amplitude matches the change in dry static stability in the simulations, implying that this theory could explain and predict the evolution of the MJO, even in the observational record that has exhibited warming.

Following this work, we investigate the temporal evolution of MJO-related precipitation and circulation amplitude and their ratio in two reanalyses (ERA5 and MERRA-2) to assess whether changes to the MJO can be detected in recent decades. A similar analysis is also applied on a century-long reanalysis (ERA-20C) to further support findings over the past few decades and to assess recent changes to the MJO in the context of low-frequency variability. Our purpose is to determine whether WTG balance can explain changes in MJO activity in the real world, which could help support projections of MJO under continued anthropogenic warming.

2. Data and Methodology

Two reanalysis data sets spanning 1981–2018 are employed to assess changes in MJO amplitude and the background environment in recent decades. The Modern-Era Retrospective analysis for Research and Applications version 2 (MERRA-2; Gelaro et al., 2017) and the European Centre for Medium-Range Weather Forecasts (ECMWF) reanalysis (ERA5; Hersbach et al., 2020) are the main data sets used to investigate MJO activity in recent decades. The ECMWF 20th century reanalysis (ERA-20C; Poli et al., 2016) is used to evaluate long-term changes in MJO behavior over 1901–2009. The MERRA-2, ERA5, and ERA-20C data sets have spatial (temporal) resolutions of $0.5^\circ \times 0.625^\circ$ (3 hours), $0.25^\circ \times 0.25^\circ$ (1 hour), and spectral truncation of T159 (1 hour), respectively. For the purpose of investigating large-scale dynamics, all variables are regridded to have a common horizontal spatial resolution of $2.5^\circ \times 2.5^\circ$. Vertical pressure velocity and precipitation are averaged into daily means, and temperature and DSE are originally obtained as monthly means. Wolding and Maloney (2015) imply that for good approximation, the slowly varying background DSE gradient is

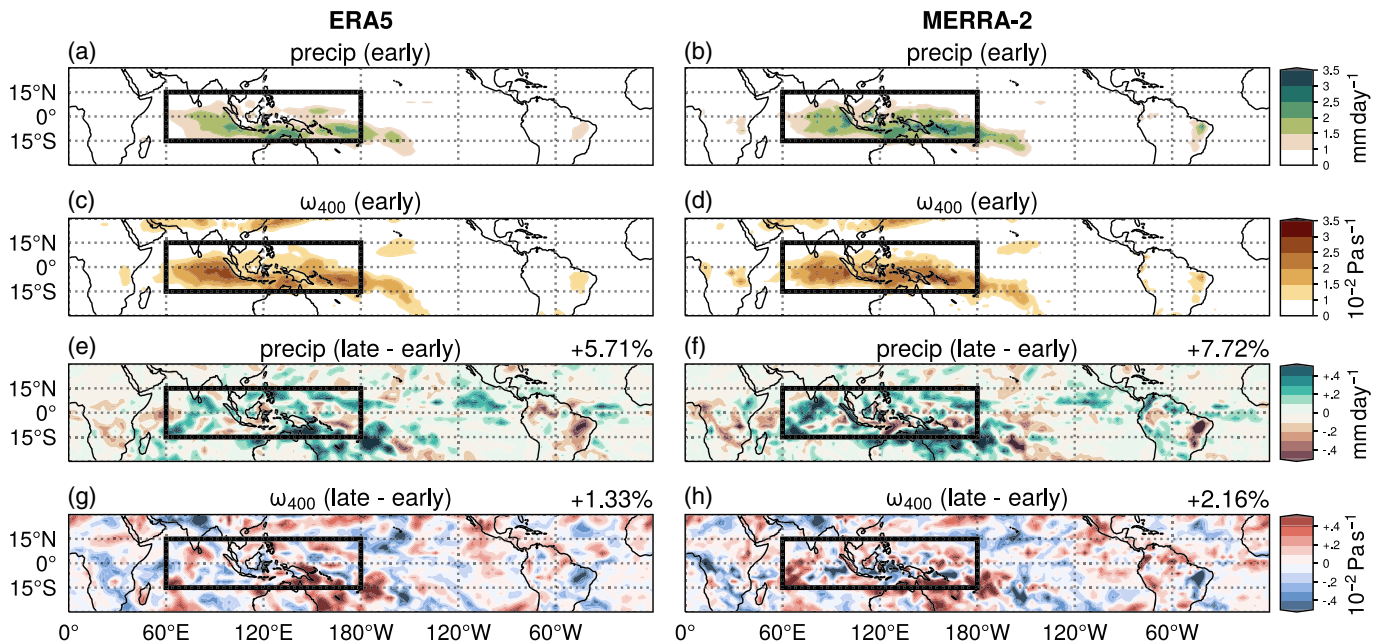


Figure 1. The boreal winter composite amplitudes of (a, b) MJO precipitation and (c, d) MJO ω_{400} during the early period (1981–1999) and (e–h) their difference from the late period (2000–2018), from (left column) ERA5 and (right column) MERRA-2. The black rectangle encloses the Indo-Pacific warm pool region, and the percentage values shown in the upper right corners of (e–h) are the area-averaged relative changes over the region.

appropriate to use in Equation 1 for determining the dominant WTG MJO balance. While the precipitation data in both reanalyses is model-generated and comes with substantial caveats, inhomogeneities in satellite-observed precipitation over the tropics make it difficult to use to detect climate trends (e.g., Yin et al., 2004). Furthermore, the moisture budget in the reanalyses products is more internally consistent, and thus, we focus on reanalysis precipitation for this work.

For ERA5 and MERRA-2, MJO activity is assessed by its associated precipitation and vertical pressure velocity amplitudes, with vertical pressure velocity at 400 hPa (ω_{400}) used given the top-heavy nature of convection in the MJO (Kiladis et al., 2005). Specifically, the occurrence of an MJO event is defined as when the magnitude of the outgoing longwave radiation-based MJO index (OMI; downloaded from NOAA PSL website; see Kiladis et al., 2014, for definition) exceeds 1.0. Note that we split our analysis into 19-year periods, and so OMI is normalized within each time period (as in Bui & Maloney, 2019) to reflect possible changes in variance of outgoing longwave radiation fields. Boreal winter (November to April) MJO composites for each of its eight phases are then generated for 30- to 90-day bandpass filtered variables as is commonly done in the MJO literature (e.g., Kiladis et al., 2014). Amplitudes of MJO precipitation and ω_{400} for each location are calculated as the root mean square values across the composites of the eight MJO phases.

Since OMI is defined by satellite OLR fields that are not available prior to 1979, MJO activity in ERA-20C is assessed using the standard deviations of precipitation and ω_{400} in the MJO band. The MJO band is defined by bandpass filtering fields to frequencies of 30–90 days and zonal wavenumbers of 1–5.

Boreal winter averages derived from monthly means of temperature and DSE are used to assess the background environment changes that could impact MJO activity. Dry static stability at 400 hPa is computed using the vertical gradient of DSE between 350 and 450 hPa.

Our focus is on the time evolution of the amplitudes of MJO precipitation and ω_{400} in the Indo-Pacific warm pool region (the IPWP region; 15°S to 15°N, 60°E to 180°) where the MJO is most active, as shown in the boxed region in Figure 1. Area-averaged MJO precipitation and ω_{400} amplitudes over the IPWP region are used as metrics to quantify overall MJO activity.

Composites obtained from 19-year running windows are extensively used in this study, similar to the averaging window length of 20 years used in Bui and Maloney (2019). This window length is chosen to reduce noise from decadal variations, but also to retain enough data points to show the time evolution of MJO activity.

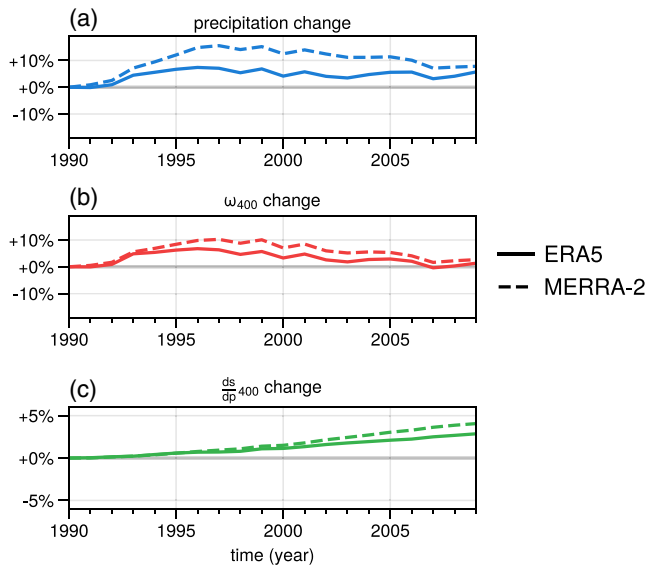


Figure 2. Relative change in 19-year wintertime running composites of (a) MJO precipitation amplitude, (b) MJO ω_{400} amplitude, and (c) dry static stability at 400 hPa with respect to the early period. The x axis denotes the central years of the associated time window, for example, 2000 denotes the period of 1991–2009. The y axis denotes the relative change to the early period.

Since the entire time period analyzed is 38 years in ERA5 and MERRA-2, the first and the last 19 years of the record are the only two periods that are truly independent, and we refer to these as the *early period* (1981–1999) and the *late period* (2000–2018). The conclusions in this study are not sensitive to the choice of window length used between 15 and 25 years (Figure S1).

Relative change (Δ) in percent is the main metric used to define changes in this study. Specifically, for any quantity X , the relative change compared to its reference state (X_{ref}) is defined by

$$\Delta(X) = \frac{X - X_{ref}}{X_{ref}} \cdot 100\% \quad (3)$$

where X_{ref} denotes the quantity over the early period (1981–1999).

3. Results

First, we explore the spatial structure of MJO activity in the two reanalyses. The amplitude of MJO precipitation and ω_{400} maximize in the IPWP region (Figures 1a–1d) in both reanalyses during the early period. The changes in MJO precipitation and ω_{400} amplitude between the late period and the early period have rich spatial structures, which are similar between the reanalyses (Figures 1e–1h). Increases in both amplitudes occur to the south of India, at the southern edge of the Pacific warm pool, and near the Philippines. Decreases in both amplitudes occur near 5°S over the Maritime Continent. The regions of large amplitude of the MJO

do not change substantially between the early and late period, allowing us to assess the temporal change in MJO activity within the IPWP region. The area-averaged amplitude of MJO precipitation and ω_{400} in the IPWP region both show increases in the late period relative to the early period with precipitation intensifying by 5.6% in ERA5 and 7.6% in MERRA-2 and ω_{400} intensifying by 1.2% in ERA5 and 2.1% in MERRA-2. Most important for this study, MJO precipitation amplitude intensifies more than MJO ω_{400} amplitude in both reanalyses, although MJO activity in MERRA-2 is strengthened slightly more than in ERA5.

The 19-year running area-averaged MJO precipitation and ω_{400} amplitude in the IPWP region increase between the early and the late periods of the record, while the amplitudes in MERRA-2 exhibit larger changes than those in ERA5. However, both reanalyses demonstrate qualitatively similar fluctuations in between: in the early 1990s, both of the amplitudes rise quickly, followed by a plateau and then a slight decrease afterward (Figures 2a and 2b). The strengthening of the boreal wintertime MJO activity during the late 20th century is consistent with previous studies examining observed zonal wind changes at 200 and 850 hPa (Jones & Carvalho, 2006). Moreover, both reanalyses agree that throughout most of the record, MJO precipitation amplitude shows larger positive changes than MJO ω_{400} amplitude.

While we attempted to explain the fluctuating pattern in MJO precipitation and ω_{400} amplitude, we could find no obvious connections between them and interannual to decadal variability in surface air temperature. The evolution of surface air temperature in the IPWP region (Figure S2b) and its evolution relative to the whole tropics (Figure S2c) do not resemble the variability in the MJO amplitude time series, which have different trends from the early 1990s onward (Figures 2a and 2b). Commonly used Pacific SST indices that capture interannual to decadal variability also do not show similar variability to the MJO amplitude time series (cf. Figures 2a and 2b with Figure S3 SST indices).

To sum up, both MJO precipitation and ω_{400} amplitude increase from the early period to the late period in the IPWP region in both reanalyses, although the time evolution is non-monotonic and the amplitude of the change varies between the reanalyses. The time series of the amplitudes are not easily explained by tropical SST variability. However, a robust result common among different time periods and reanalyses is that the increase in MJO precipitation amplitude is always stronger than in MJO ω_{400} amplitude, consistent with what WTG balance would predict based on the increasing tropical static stability with SST warming observed in recent decades (Figure 2c; see also e.g., Sherwood & Nishant, 2015). We explore this contention more below.

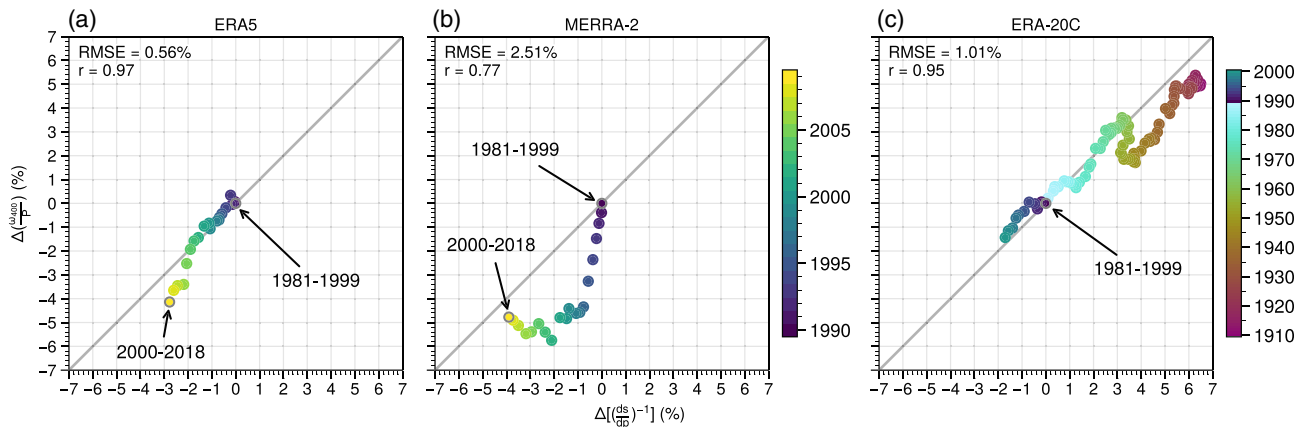


Figure 3. Relative change in (x axis) the reciprocal of dry static stability at 400 hPa and (y axis) the ratio of MJO ω_{400} to precipitation amplitude over the IPWP region between 19-year running windows and the early period. Colors indicate the central year of the running window. The gray diagonal line denotes the change in the ratio predicted by WTG balance assuming vertical heating structure is unchanged (Equation 2). Root mean square errors (RMSEs) of MJO ω_{400}/P relative to theoretical predictions are provided in each panel. Correlation coefficients (r) between the two variables are also provided to show how coherent they change. Note that the MJO-associated quantities are defined using OMI for (a) ERA5 and (b) MERRA-2, whereas standard deviations in the MJO wavenumber-frequency band are used for (c) ERA-20C.

Given a change in dry static stability, the theoretical change in the ratio of MJO ω_{400} to precipitation amplitude can be computed if one assumes that WTG balance holds (Equation 1) and that the vertical structure of Q_1 associated with the MJO is not changed (Equation 2). Previous modeling studies have shown good agreement between static stability changes and this ratio when applied to MJO-associated wind and precipitation variance (Bui & Maloney, 2018; Maloney & Xie, 2013; Wolding et al., 2016; Wolding & Maloney, 2015). As the climate system warms, tropical dry static stability increases in the troposphere because the atmospheric profile in the deep tropics roughly follows a moist adiabat set by the surface temperature in convecting regions (Knutson & Manabe, 1995). Consistently, increasing dry static stability has been observed in recent years as surface temperature has increased (Allen & Sherwood, 2008). Because surface temperature has increased since 1981 (Figure S2a), Equation 2 would argue for a greater change in MJO precipitation amplitude compared to MJO ω_{400} amplitude.

Figures 3a and 3b display the temporal evolution of the inverse of dry static stability and the ratio of MJO ω_{400} to precipitation amplitude (MJO ω_{400}/P ; see Equation 2) in ERA5 and MERRA-2. The gray diagonal line denotes the predicted theoretical relationship between MJO ω_{400}/P and inverse static stability assuming WTG theory holds and the vertical structure of the MJO remains unchanged. Between the late period and the early period (the two outlined endpoints), the decrease of the inverse of dry static stability is 2.8% in ERA5 and 4.0% in MERRA-2, and the decrease of MJO ω_{400}/P is 4.2% in ERA5 and 4.9% in MERRA-2. Consistent with WTG theory, MJO ω_{400}/P and the inverse of dry static stability show comparable decreases between the early period (1981–1999) and the late period (2000–2018). Agreement is also good in ERA5 for interim periods, especially until about 2000 (Figure 3a). Considering the complicated temporal evolution of MJO precipitation and ω_{400} amplitude (Figure 2), WTG balance provides a reasonable explanation for the evolution of MJO ω_{400}/P over the past 38 years, especially when considering the start and end of the record.

As many MJO studies use zonal wind amplitude as a metric of MJO activity (e.g., Jones & Carvalho, 2006; Slingo et al., 1999), we also examine the amplitude of MJO 850-hPa zonal wind (u_{850}) for reference. The evolution of the ratio of MJO circulation to precipitation amplitude is defined here using u_{850} (MJO u_{850}/P). Although using u_{850} is not a direct application of WTG balance in Equation 2, the amplitude of horizontal velocity should scale with vertical velocity through divergence if the vertical structure doesn't change (Maloney & Xie, 2013). Under such conditions, we would expect a qualitatively similar decrease in the ratio of MJO u_{850} to precipitation amplitude. Figure S4 shows that u_{850} amplitude relative to precipitation does decrease in a qualitatively similar way, although with stronger decreases relative to P than for ω_{400} .

Although MJO ω_{400}/P generally follows the change in the inverse of dry static stability, there exist deviations from theoretical predictions, with maximum differences of about 1.5% in ERA5 and 4% in MERRA-2. To place these values in a larger-scale context, we compare Figures 3a and 3b to Figure 3c that shows

results from ERA-20C spanning 1901–2009. The theoretical estimate works well in ERA-20C over the whole century, with about 7–8% decreases in both MJO ω_{400}/P and inverse static stability over the century. The maximum deviation of MJO ω_{400}/P change in ERA-20C is about 2% from theoretical values predicted by the inverse of dry static stability. Deviations of ERA5 from theoretical values are even smaller than this, while deviations in MERRA-2 are larger. As described below, deviations of MERRA-2 from the theoretical estimate may occur due to the imperfect assumption of proportionality of Q_1 at 400 hPa and P .

In MERRA-2, Equation 2 overestimates the decrease in MJO ω_{400}/P in the intervening periods but works well for the two endpoints. MJO ω_{400}/P in MERRA-2 shows stronger decreases than ERA5 during the interim period largely because it has a larger P amplitude change than ERA5. The exact reasons for differences between the two analyses are unclear, although they may depend on the different behavior of tropical convection simulated by the two reanalysis models. The differing DSE profile changes between ERA5 and MERRA-2 for the IPWP region (Figure S5) not only indicate differing static stability changes but also circumstantially suggest different changes to the convective heating structure between data sets given the regulation of tropical tropospheric temperature by convective heating. Such structure changes would affect how well the balance in Equation 2 reflects Equation 1, considering the assumption about the proportionality of P to Q_1 at 400 hPa. MERRA-2 exhibits more warming in the lower troposphere than ERA5, presumably associated with increased condensational heating and precipitation generation there, which would produce greater decreases in MJO ω_{400}/P than that expected by looking at the 400 hPa level in isolation. The rate of increase in low-level warming in MERRA-2 is particularly strong until the 19-year period centered on 1997, possibly consistent with the greater MJO precipitation amplitude increase in MERRA-2 during that time than ERA5 (Figure 2), although translating mean state convective structure changes to those on subseasonal timescales should be done with care.

An examination of MJO anomaly amplitudes of Q_1 at 400 hPa and precipitation suggests a weaker consistency between the two quantities in MERRA-2 (Figure S6), consistent with possible vertical structure changes. However, while the change in the ratio of ω_{400} to Q_1 amplitude at 400 hPa generally follows dry static stability in ERA5, the agreement is not as good as in MERRA-2 (Figure S7), which might also explain some of the differing behavior in Figure 3. The reasons for this discrepancy are unclear.

4. Summary

The changes to MJO precipitation and ω_{400} amplitude from 1981 to 2018 are examined in three reanalysis data sets: ERA5, MERRA-2, and ERA-20C. Both amplitudes in ERA5 and MERRA-2 individually increased from the early period (1981–1999) to the late period (2000–2018) (Figure 1). However, their temporal behavior is non-monotonic in that both amplitudes intensify from 1981 to 1997 and slowly weaken or remain constant thereafter (Figures 2a and 2b). Interannual-to-decadal surface temperature variability (Figures S2 and S3) shows no simple relationship with this non-monotonic behavior in MJO activity changes.

When viewed together, amplitude changes of MJO precipitation are larger than MJO ω_{400} throughout the past four decades relative to the early period (1981–1999). A preferential strengthening of MJO precipitation amplitude relative to MJO ω_{400} amplitude is predicted by WTG balance with a warming climate, in that increasing dry static stability in response to SST warming in recent decades makes vertical motion more efficient at compensating latent heat release in deep convective regions. The fractional amplitude changes in the ratio of MJO ω_{400} to precipitation between 1981–1999 and 2000–2018 approximately match inverse dry static stability changes with climate warming, consistent with WTG balance (Figures 3a and 3b). A similar result is shown in ERA-20C between 1901–1919 and 1991–2009 (Figure 3c).

While trends in these reanalyses appear to generally follow WTG balance, differences exist in the behavior of the three reanalyses. MJO precipitation and ω_{400} amplitude increases are larger in MERRA-2 than in ERA5, especially in intermediate periods between the beginning and end of the record, although they show qualitatively similar time series variability (Figure 2). Decreases in MJO ω_{400}/P also fit the theoretical prediction based on the inverse of dry static stability better in ERA5 and ERA-20C than in MERRA-2 across all 19-year periods examined in terms of RMSE, and these differences may be associated with differences in the simulated structure of tropical deep convection, which remains a topic for further investigation.

The present paper provides a preliminary assessment of MJO activity changes in precipitation and vertical velocity over the past four decades that include both anthropogenic forcing and natural variability and uses a

century-long data set to assess recent changes in the context of natural variability over the longer record. Our results based on observations support those previously derived from climate models (e.g., Bui & Maloney, 2019) suggesting that decreases in MJO ω_{400}/P occur as surface temperatures warm due to anthropogenic forcing. Nevertheless, discrepancies between results from ERA5 and MERRA-2 leave lingering questions about the degree to which changes to the MJO can be explained by WTG theory, including the assumption that Q_1 has no vertical structural changes in response to climate warming. Further work using a broader set of observational data including tropical sounding and other in situ records is needed to affirm the validity of Equation 2 for explaining MJO behavior.

Data Availability Statement

Data can be accessed online (ERA5: <https://cds.climate.copernicus.eu>; MERRA-2: https://gmao.gsfc.nasa.gov/reanalysis/MERRA-2/data_access; ERA-20C: <https://www.ecmwf.int/en/forecasts/datasets/reanalysis-datasets/era-20c>; OMI: <https://www.psl.noaa.gov/mjo/mjoindex>; Niño 3.4: <https://climatedataguide.ucar.edu/climate-data/nino-sst-indices-nino-12-3-34-4-oni-and-tni>; PDO index: <https://www.ncdc.noaa.gov/teleconnections/pdo>; and TPI: <https://psl.noaa.gov/data/timeseries/IPOTPI>).

Acknowledgments

This research has been conducted as part of the NOAA MAPP S2S Prediction Task Force and supported by NOAA grant NA16OAR4310064 as well as NOAA OWAQ grant NA19OAR4590151. Work was also supported by NSF grant AGS-1841754.

References

- Allen, R. J., & Sherwood, S. C. (2008). Warming maximum in the tropical upper troposphere deduced from thermal winds. *Nature Geoscience*, *1*(6), 399–403. <https://doi.org/10.1038/ngeo208>
- Arnold, N. P., Kuang, Z., & Tziperman, E. (2013). Enhanced MJO-like variability at high SST. *Journal of Climate*, *26*(3), 988–1001. <https://doi.org/10.1175/JCLI-D-12-00272.1>
- Bui, H. X., & Maloney, E. D. (2018). Changes in Madden Julian oscillation precipitation and wind variance under global warming. *Geophysical Research Letters*, *45*, 7148–7155. <https://doi.org/10.1029/2018GL078504>
- Bui, H. X., & Maloney, E. D. (2019). Transient response of MJO precipitation and circulation to greenhouse gas forcing. *Geophysical Research Letters*, *46*, 13,546–13,555. <https://doi.org/10.1029/2019GL085328>
- Chikira, M. (2014). Eastward-propagating intraseasonal oscillation represented by Chikira–Sugiyama cumulus parameterization. Part II: Understanding moisture variation under weak temperature gradient balance. *Journal of the Atmospheric Sciences*, *71*(2), 615–639. <https://doi.org/10.1175/JAS-D-13-038.1>
- Ferranti, L., Palmer, T. N., Molteni, F., & Klinker, E. (1990). Tropical-extratropical interaction associated with the 30–60 day oscillation and its impact on medium and extended range prediction. *Journal of the Atmospheric Sciences*, *47*(18), 2177–2199. [https://doi.org/10.1175/1520-0469\(1990\)047<2177:TEIAWT>2.0.CO;2](https://doi.org/10.1175/1520-0469(1990)047<2177:TEIAWT>2.0.CO;2)
- Gelaro, R., McCarty, W., Suárez, M. J., Todling, R., Molod, A., Takacs, L., et al. (2017). The Modern-Era retrospective analysis for research and applications, version 2 (MERRA-2). *Journal of Climate*, *30*(Iss 13), 5419–5454. <https://doi.org/10.1175/JCLI-D-16-0758.1>
- Hersbach, H., Bell, B., Berrisford, P., Hirahara, S., Horányi, A., Muñoz Sabater, J., et al. (2020). The ERA5 global reanalysis. *Quarterly Journal of the Royal Meteorological Society*, *64*, 29. <https://doi.org/10.1002/qj.3803>
- Holloway, C. E., & Neelin, J. D. (2009). Moisture vertical structure, column water vapor, and tropical deep convection. *Journal of the Atmospheric Sciences*, *66*(6), 1665–1683. <https://doi.org/10.1175/2008JAS2806.1>
- Jones, C., & Carvalho, L. M. V. (2006). Changes in the activity of the Madden-Julian oscillation during 1958–2004. *Journal of Climate*, *19*(24), 6353–6370. <https://doi.org/10.1175/JCLI3972.1>
- Kiladis, G. N., Dias, J., Straub, K. H., Wheeler, M. C., Tulich, S. N., Kikuchi, K., et al. (2014). A comparison of OLR and circulation-based indices for tracking the MJO. *Monthly Weather Review*, *142*(5), 1697–1715. <https://doi.org/10.1175/mwr-d-13-00301.1>
- Kiladis, G. N., Straub, K. H., & Haertel, P. T. (2005). Zonal and vertical structure of the Madden-Julian oscillation. *Journal of the Atmospheric Sciences*, *62*(8), 2790–2809. <https://doi.org/10.1175/JAS3520.1>
- Knutson, T. R., & Manabe, S. (1995). Time-mean response over the tropical pacific to increased CO₂ in a coupled ocean-atmosphere model. *Journal of Climate*, *8*(9), 2181–2199. [https://doi.org/10.1175/1520-0442\(1995\)008<2181:TMROTT>2.0.CO;2](https://doi.org/10.1175/1520-0442(1995)008<2181:TMROTT>2.0.CO;2)
- Madden, R. A., & Julian, P. R. (1971). Detection of a 40–50 day oscillation in the zonal wind in the tropical Pacific. *Journal of the Atmospheric Sciences*, *28*(5), 702–708. [https://doi.org/10.1175/1520-0469\(1971\)028<0702:DOADOI>2.0.CO;2](https://doi.org/10.1175/1520-0469(1971)028<0702:DOADOI>2.0.CO;2)
- Madden, R. A., & Julian, P. R. (1972). Description of global-scale circulation cells in the tropics with a 40–50 day period. *Journal of the Atmospheric Sciences*, *29*(6), 1109–1123. [https://doi.org/10.1175/1520-0469\(1972\)029<1109:DOGSCC>2.0.CO;2](https://doi.org/10.1175/1520-0469(1972)029<1109:DOGSCC>2.0.CO;2)
- Maloney, E. D., Adames, A. F., & Bui, H. X. (2019). Madden-Julian oscillation changes under anthropogenic warming. *Nature Climate Change*, *9*(1), 26–33. <https://doi.org/10.1038/s41558-018-0331-6>
- Maloney, E. D., & Xie, S.-P. (2013). Sensitivity of tropical intraseasonal variability to the pattern of climate warming: MJO activity and climate warming. *Journal of Advances in Modeling Earth Systems*, *5*, 32–47. <https://doi.org/10.1029/2012MS000171>
- Oliver, E. C. J., & Thompson, K. R. (2012). A reconstruction of Madden-Julian oscillation variability from 1905 to 2008. *Journal of Climate*, *25*(6), 1996–2019. <https://doi.org/10.1175/JCLI-D-11-00154.1>
- Poli, P., Hersbach, H., Dee, D. P., Berrisford, P., Simmons, A. J., Vitart, F., et al. (2016). ERA-20C: An atmospheric reanalysis of the twentieth century. *Journal of Climate*, *29*(11), 4083–4097. <https://doi.org/10.1175/JCLI-D-15-0556.1>
- Sherwood, S. C., & Nishant, N. (2015). Atmospheric changes through 2012 as shown by iteratively homogenized radiosonde temperature and wind data (IUKv2). *Environmental Research Letters*, *10*(5), 054007. <https://doi.org/10.1088/1748-9326/10/5/054007>
- Slingo, J. M., Rowell, D. P., Sperber, K. R., & Nortley, F. (1999). On the predictability of the interannual behaviour of the Madden-Julian oscillation and its relationship with El Niño. *Quarterly Journal of the Royal Meteorological Society*, *125*(554), 583–609. <https://doi.org/10.1002/qj.49712555411>
- Sobel, A. H., & Bretherton, C. S. (2000). Modeling tropical precipitation in a single column. *Journal of Climate*, *13*(24), 4378–4392. [https://doi.org/10.1175/1520-0442\(2000\)013<4378:MTPIAS>2.0.CO;2](https://doi.org/10.1175/1520-0442(2000)013<4378:MTPIAS>2.0.CO;2)
- Tao, L., Zhao, J., & Li, T. (2015). Trend analysis of tropical intraseasonal oscillations in the summer and winter during 1982–2009: Trend analysis of BSISO and MJO during 1982–2009. *International Journal of Climatology*, *35*(13), 3969–3978. <https://doi.org/10.1002/joc.4258>

- Wolding, B. O., & Maloney, E. D. (2015). Objective diagnostics and the Madden-Julian oscillation. Part II: Application to moist static energy and moisture budgets. *Journal of Climate*, 28(19), 7786–7808. <https://doi.org/10.1175/JCLI-D-14-00689.1>
- Wolding, B. O., Maloney, E. D., & Branson, M. (2016). Vertically resolved weak temperature gradient analysis of the Madden-Julian oscillation in SP-CESM. *Journal of Advances in Modeling Earth Systems*, 8, 1586–1619. <https://doi.org/10.1002/2016MS000724>
- Yanai, M., Esbensen, S., & Chu, J.-H. (1973). Determination of bulk properties of tropical cloud clusters from large-scale heat and moisture budgets. *Journal of the Atmospheric Sciences*, 30(4), 611–627. [https://doi.org/10.1175/1520-0469\(1973\)030<0611:DOBPOT>2.0.CO;2](https://doi.org/10.1175/1520-0469(1973)030<0611:DOBPOT>2.0.CO;2)
- Yin, X., Gruber, A., & Arkin, P. (2004). Comparison of the GPCP and CMAP merged Gauge–Satellite monthly precipitation products for the period 1979–2001. *Journal of Hydrometeorology*, 5(6), 1207–1222. <https://doi.org/10.1175/JHM-392.1>
- Zhang, C. (2013). Madden-Julian oscillation: Bridging weather and climate. *Bulletin of the American Meteorological Society*, 94(12), 1849–1870. <https://doi.org/10.1175/BAMS-D-12-00026.1>